**Journal of Pathology**
*J Pathol* April 2023; **259:** 402–414
Published online 17 February 2023 in Wiley Online Library
(wileyonlinelibrary.com) DOI: 10.1002/path.6053

ORIGINAL ARTICLE

# Anti-CD40L therapy prevents the formation of precursor lesions to gastric B-cell MALT lymphoma in a mouse model

Le Ying[1,2], Phoebe Liu[3], Zhoujie Ding[4,5], Georgie Wray-McCann[1], Jack Emery[1], Nina Colon[1], Lena HM Le[1], Le Son Tran[1], Ping Xu[6], Liang Yu[7], Dana J Philpott[3], Yugang Tu[8], Daryl MZ Cheah[9], Chee L Cheng[10], Soon T Lim[11,12,13], Choon K Ong[9,14,15] and Richard L Ferrero[1,2,16]*

[1] *Centre for Innate Immunity and Infectious Diseases, Hudson Institute of Medical Research, Clayton, VIC, Australia*
[2] *Department of Molecular and Translational Science, Monash University, Clayton, VIC, Australia*
[3] *Department of Immunology, University of Toronto, Toronto, ON, Canada*
[4] *Department of Immunology and Pathology, Central Clinical School, Monash University, Clayton, VIC, Australia*
[5] *Department of Microbiology, Tumor and Cell Biology, Karolinska Institutet, Solna, Sweden*
[6] *Department of Tea Science, Zhejiang University, Hangzhou, PR China*
[7] *Department of General Surgery, Shanghai General Hospital, Shanghai Jiao Tong University School of Medicine, Shanghai, PR China*
[8] *Cell Signaling Technology, Inc., Danvers, MA, USA*
[9] *Lymphoma Genomic Translational Research Laboratory, Cellular and Molecular Research, National Cancer Centre Singapore, Singapore, Singapore*
[10] *Department of Pathology, Singapore General Hospital, Singapore, Singapore*
[11] *Division of Medical Oncology, National Cancer Centre Singapore, Singapore, Singapore*
[12] *SingHealth Duke-NUS Blood Cancer Centre, Singapore, Singapore*
[13] *Office of Education, Duke-NUS Medical School, Singapore, Singapore*
[14] *Cancer and Stem Cell Biology Program, Duke-NUS Medical School, Singapore, Singapore*
[15] *Genome Institute of Singapore, Singapore, Singapore*
[16] *Biomedicine Discovery Institute, Department of Microbiology, Monash University, Clayton, VIC, Australia*

*Correspondence to: RL Ferrero, Centre for Innate Immunity and Infectious Diseases, Hudson Institute of Medical Research, 27–31 Wright Street, Clayton, Melbourne, Victoria 3168, Australia. E-mail: richard.ferrero@hudson.org.au

## Abstract

**Mucosa-associated lymphoid tissue (MALT) lymphoma is a B-cell tumour that develops over many decades in the stomachs of individuals with chronic *Helicobacter pylori* infection. We developed a new mouse model of human gastric MALT lymphoma in which mice with a myeloid-specific deletion of the innate immune molecule, Nlrc5, develop precursor B-cell lesions to MALT lymphoma at only 3 months post-*Helicobacter* infection versus 9–24 months in existing models. The gastric B-cell lesions in the *Nlrc5* knockout mice had the histopathological features of the human disease, notably lymphoepithelial-like lesions, centrocyte-like cells, and were infiltrated by dendritic cells (DCs), macrophages, and T-cells ($CD4^+$, $CD8^+$ and $Foxp3^+$). Mouse and human gastric tissues contained immune cells expressing immune checkpoint receptor programmed death 1 (PD-1) and its ligand PD-L1, indicating an immunosuppressive tissue microenvironment. We next determined whether CD40L, overexpressed in a range of B-cell malignancies, may be a potential drug target for the treatment of gastric MALT lymphoma. Importantly, we showed that the administration of anti-CD40L antibody either coincident with or after establishment of *Helicobacter* infection prevented gastric B-cell lesions in mice, when compared with the control antibody treatment. Mice administered the CD40L antibody also had significantly reduced numbers of gastric DCs, $CD8^+$ and $Foxp3^+$ T-cells, as well as decreased gastric expression of B-cell lymphoma genes. These findings validate the potential of CD40L as a therapeutic target in the treatment of human gastric B-cell MALT lymphoma.**



**Keywords:** CD40 ligand; BAFF; APRIL; B-cell; MALT lymphoma; PD-L1; multiplex immunohistochemistry; NLRC5; *Helicobacter*

Received 1 August 2022; Revised 21 December 2022; Accepted 11 January 2023

*No conflicts of interest were declared.*

## Introduction

Gastric B-cell mucosa-associated lymphoid tissue (MALT) lymphoma is one of the most common non-Hodgkin lymphomas, accounting for 7–8% of newly diagnosed lymphoma cases worldwide [1]. The stomach is the most affected site, accounting for 50–60% of all MALT lymphomas in Western countries [2]. In up to 98% of diagnosed cases, gastric MALT lymphoma is associated with *Helicobacter pylori* infection [3].

Currently, the first-line therapy for early-stage gastric MALT lymphoma is *H. pylori* eradication; however, relapse was reported in 17% (13/74) of MALT subjects at 75 months post-eradication [4]. More advanced disease is typically treated by radiotherapy, chemotherapy, or surgery [5,6]. Again, however, relapse occurred in 37% of MALT subjects at between 14 and 307 months after complete remission [7], with 18% (6/33) relapsing after 10 years [8].

The drug rituximab targets CD20 on mature B-cells, resulting in their elimination [6]. This drug has been widely used as a single agent or in combination with chemotherapies to treat various types of non-Hodgkin lymphoma, including *Helicobacter*-associated gastric MALT lymphoma [6,9]. One study, however, reported that ∼27% patients with MALT lymphoma did not respond to this treatment, while a further 26% of patients relapsed during a 15-month follow-up period [9]. Therefore, more therapeutic options are needed.

B-cells express the tumour necrosis factor (TNF) receptor superfamily member CD40 [10], which interacts with its ligand, CD40L, on activated T-cells to promote B-cell differentiation, activation, and proliferation [11]. Dysregulation of CD40–CD40L signalling contributes to B-cell lymphomagenesis [11]. Greiner *et al* reported that CD40L signalling, in combination with T-helper 2 (Th2) cytokines, may drive the evolution of low-grade MALT-type lymphoma to a more severe stage [12]. In contrast, other researchers found that *Helicobacter*-induced MALT lymphomagenesis occurred independently of direct CD40–CD40L interactions [13]. Both studies, however, were performed using MALT lymphoma B-cells grown *in vitro*. To date, there have been no reports on the *in vivo* effects of CD40–CD40L blockade in *Helicobacter*-induced gastric MALT lymphoma.

Many of the features of human gastric B-cell MALT lymphoma can be reproduced in conventional mice that have been experimentally infected with gastric *Helicobacter* spp. [14–17]. These mice, however, develop gastric B-cell MALT after 6–18 months post-infection [14–17]. Our group has developed a mouse model in which animals develop B-cell follicles after only 3 months post-infection with *Helicobacter felis* [18]. These mice have a myeloid-specific deletion of the gene encoding the innate immune molecule, NLR family CARD domain-containing 5 (*Nlrc5*) [18].

Myeloid cells secret cytokines that drive the polarisation of Th responses, including Th1, Th2, and Th17. These responses have variously been reported to be associated with gastric MALT lymphomagenesis in different experimental models [19]. As one of the major subgroups of myeloid cells, macrophages also secrete B-cell survival regulators, such as a proliferation-inducing ligand (APRIL or TNF ligand superfamily member 13, TNFSF13) and B-cell-activating factor (BAFF or TNFSF13B) [20]. Soluble APRIL and BAFF bind to their receptors on B-cells and lead to the activation of B-cells [21]. These proteins share two receptors on B-cells: B-cell maturation antigen (BCMA or TNF receptor superfamily member 17, TNFRSF17) and transmembrane activator and calcium-modulating cyclophilin ligand interactor (TACI or TNFRSF13B). BAFF can also bind to a third receptor, BAFF-R (or TNFRSF13C) [20]. However, the role of these B-cell survival factors in gastric MALT lymphomagenesis is still not clear.

In the current study, we performed multiplex immunohistochemistry (mIHC) to compare B-cell MALT lesions in *Helicobacter*-infected *Nlrc5* conditional knockout ($Nlrc5^{mø\text{-}KO}$) mice with those in human gastric B-cell MALT lymphoma. We show that the $Nlrc5^{mø\text{-}KO}$ mouse model reproduces the key histopathological characteristics of the tumours observed in human disease. Using this model, we tested the efficacy of CD40L blockade in preventing the formation of the precursor lesions to these tumours. Importantly, we show that anti-CD40L antibody administration both during and after establishment of chronic infection was an effective treatment against the development of these lesions. We propose that the CD40–CD40L axis is a potential therapeutic target for the treatment of human gastric B-cell MALT lymphoma arising from chronic *H. pylori* infection.

## Materials and methods

### Mice

Mice with an *Nlrc5* deletion in the myeloid lineage ($Nlrc5^{mø\text{-}KO}$) [18] were maintained under specific pathogen-free conditions at Monash Animal Research Platform, Monash Medical Centre (MMC). All animal procedures complied with the guidelines approved by the MMC Animal Ethics Committee (MMCB/2017/13).

### Human gastric MALT lymphoma biopsies

Gastric MALT lymphoma biopsies were collected from consenting participants ($n = 5$) in accordance with the Declaration of Helsinki with approval from the Institutional Review Boards from SingHealth (2004/407/F). Clinical work at the Hudson Institute was approved by the Monash Health Human Research Ethics Committee (HREC, 12365A; Monash University HREC, CF13/2974 – 2013001598). Tissues were formalin-fixed and paraffin-embedded. The presence of *H. pylori* and MALT lymphoma lesions were confirmed in haematoxylin and eosin (H&E)-stained sections (see supplementary material, Figure S1A–C). Representative H&E staining of gastric MALT lymphoma lesions from five human cases are shown in supplementary material, Figure S2.

### Bacterial culture

*H. felis* (ATCC 49179/CS1) was grown and maintained using standard methods [22]. For *in vivo* infection, *H. felis* inocula were prepared in Brain Heart Infusion (BHI) broth [22]. The number of bacteria was estimated under phase contrast microscopy (100× objective) and then diluted to approximately $10^8$ bacteria/ml in BHI

broth [22]. *H. felis* bacterial numbers were confirmed by viable bacterial cell counting [22].

### Anti-CD40L treatment studies

*Nlrc5*$^{mø\text{-}KO}$ mice (female; 6–8 weeks of age) were inoculated by oral gavage with approximately $10^7$ *H. felis* bacteria [22]. In one treatment regimen, mice were administered an intraperitoneal injection at the time of *H. felis* inoculation with either anti-mouse CD40L ($n = 11$, 200 µg/dose; BioXCell, West Lebanon, NH, USA) or IgG control ($n = 10$, 200 µg/dose, BioXCell) antibodies, followed by weekly intraperitoneal injections over 12 weeks (supplementary material, Figure S3A). In a second treatment regimen, mice were first inoculated with *H. felis* and then 1 month later, they were administered weekly intraperitoneal injections with either anti-mouse CD40L ($n = 7$) or IgG control ($n = 6$) antibodies, for a further 8 weeks (supplementary material, Figure S3B). After 12 weeks, all mice were culled. Stomach tissues were dissected into two sagittal fragments (each containing the antrum and body); one half was used for mIHC and the other half for RNA extraction. Spleens and mesenteric lymph nodes were used to determine the percentage of immune cells by flow cytometry. Sera were used for enzyme-linked immunosorbent assay (ELISA).

### H&E and Giemsa staining

Gastric tissues were deparaffinised, stained with H&E for 5 min, and then scanned using a VS120 Slide Scanning System (Olympus, Tokyo, Japan). The results were quantified in a blinded fashion using QuPath software [23]. As *H. felis* does not form discrete colonies on agar plates [24], colonisation levels in the stomach were determined from Giemsa-stained sections that were examined in a blinded fashion using a scoring system described previously [25].

### Multiplex immunohistochemistry (mIHC)

mIHC was applied using the Opal 4-Color IHC Kit (Akoya Biosciences, Menlo Park, CA, USA), as described previously [26] (supplementary material, Table S1). Tissue sections were deparaffinised and subjected to antigen retrieval by microwave treatment. The sections were incubated in blocking buffer, primary antibody (supplementary material, Table S1), horseradish peroxidase (Cell Signaling Technology, Beverly, MA, USA), and Opal working solution (Akoya Biosciences). DAPI (Akoya Biosciences) was used to stain the nuclei. Slides were scanned using a VS120 Slide Scanning System (Olympus) and quantified in a blinded fashion using ImageJ software (National Institutes of Health, Bethesda, MD, USA; https://imagej.net/ij/download.html).

### Flow cytometric analysis

Single-cell suspensions were prepared from spleens and mesenteric lymph nodes using 70-µm cell strainers. Splenocytes were treated with red blood cell lysis buffer (Sigma Aldrich, St Louis, MO, USA). Cell numbers and viability were assessed using a haemocytometer. Cells were first incubated with Fc block (BioLegend, San Diego, CA, USA) and then stained with two different antibody panels: panel 1: CD19, CD3, CD4, CD8a, B220, and CD45; or panel 2: CD11c, CD11b, F4/80, MHCII, Ly6C, Ly6G, and CD45 (supplementary material, Table S2). Cells were analysed using a BD LSRFortessa X-20 flow cytometer (BD Biosciences, San José, CA, USA) and FlowJo software (Version 10; Treestar, Inc., San Carlos, CA, USA). The gating strategies for the different cell populations are shown in supplementary material, Figure S4.

### ELISA

Sera were collected in Sarstedt Screw Cap Polypropylene Microtubes (Thermo Fisher Scientific, Waltham, MA, USA) and stored at −20 °C until analysed. *Helicobacter*-specific serum antibody titres were measured by ELISA, as described previously [27], using goat anti-mouse IgG (1:2,000; BioLegend), goat anti-mouse IgG2c-biotin (1:1,000; Southern Biotech, Birmingham, AL, USA), and rat anti-mouse IgG1-biotin (1:1,000; Southern Biotech) antibodies.

### RT-qPCR

Total RNA was extracted from snap-frozen mouse stomachs using a PureLink RNA Mini Kit and Turbo-DNase following the manufacturer's instructions (Thermo Fisher Scientific). Complementary DNA was generated from RNA using a Tetro cDNA Synthesis Kit (Bioline, Eveleigh, NSW, Australia). qPCR was performed with gene-specific primers (supplementary material, Table S3) or Taqman probes (supplementary material, Table S4) in a QuantStudio 6 Flex Real-Time PCR instrument (Applied Biosystems, Waltham, MA, USA). Relative gene expression levels in samples were determined using the delta–delta Ct ($2^{-\Delta\Delta Ct}$) method with ΔCt values normalised to those of *Rn18s* ribosomal RNA.

### Statistical analyses

Statistical analyses in this study were carried out using the Mann–Whitney test in Prism (Version 9.0; GraphPad Software Inc., San Diego, CA, USA). Data are reported as the mean ± standard error of the mean (SEM). *P* values less than 0.05 were considered as statistically significant.

## Results

### *Nlrc5*$^{mø\text{-}KO}$ mice with chronic *Helicobacter* infection reproduce the histopathological features of human gastric MALT lymphoma

Our previous work demonstrated that *Nlrc5*$^{mø\text{-}KO}$ mice develop lymphoid structures or follicles within the gastric mucosa by only 12 weeks post-*H. felis* infection, compared with much longer periods in wild-type animals, i.e. up to 24 months [18]. To determine whether

*Nlrc5*$^{mø\text{-}KO}$ mice can be used as a model of human gastric B-cell MALT lymphomagenesis, we performed a detailed comparative study of the MALT lesions in these animals and those in human subjects with gastric MALT lymphoma. The lymphoid follicles in both *Nlrc5*$^{mø\text{-}KO}$ mice with MALT and human subjects with gastric MALT lymphoma span the gastric mucosa (Figure 1A,B). These follicles are infiltrated by lympho-epithelial lesions and small- to medium-sized centrocyte-like cells having small and irregular nuclei (Figure 1C,D), which are hallmarks of human MALT lymphoma [28]. Dramatically increased numbers of centrocyte-like cells were observed in the gastric tissues of mice with MALT lesions, whereas no centrocyte-like cells were found in the stomachs of naïve animals (supplementary material, Table S5). Furthermore, the B-cell follicles in mouse and human gastric tissues were infiltrated with a predominance of CD21$^+$ B-cells (Figure 1E,F) and some IgM$^+$ B-cells (supplementary material, Figure S5). Interestingly, there was also a preponderance of Ki67$^+$ cells in B-cell follicles (supplementary material, Figure S6), suggesting that these cells were proliferative. Taken together, we suggest that *H. felis*-infected *Nlrc5*$^{mø\text{-}KO}$ mice exhibit the phenotype of early marginal zone B-cell lymphoma.

Next, we compared the cellular composition and microenvironment of the gastric MALT lesions in *H. felis*-infected *Nlrc5*$^{mø\text{-}KO}$ mice and those in human MALT lymphoma by mIHC. As for human gastric MALT lesions, those in mice are predominately composed of B-cells and CD11c$^+$ dendritic cells (DCs), surrounded or infiltrated by large numbers of macrophages (Figure 1G,H and supplementary material, Figure S7). Abundant numbers of CD4$^+$ and CD8$^+$ T-cells were present in mouse and human tissues, along with the infiltration of Foxp3$^+$ T regulatory cells (Tregs) (Figure 1I,J). The relative abundance of CD4$^+$ T-cells compared with Foxp3$^+$ T-cells was quite similar in both mouse and human tissues, whereas the ratio of CD8$^+$ T-cells to Foxp3$^+$ T-cells was slightly higher in human tissues than in mouse tissues (supplementary material, Figure S8). All the Tregs were confirmed to be CD4$^+$ T-cells (supplementary material, Figure S9). Consistent with previous reports showing the presence in B-cell MALT lymphoma of high levels of expression of the immune checkpoint receptor programmed death 1 (PD-1) and its ligand PD-L1 [29,30], we detected the expression by immune cells within both mouse and human gastric tissues (Figure 1K,L). Tissue infiltration by Foxp3$^+$ Tregs and PD-1/PD-L1 expression are indicative of an immunosuppressive microenvironment. Collectively, these data show that the *Nlrc5*$^{mø\text{-}KO}$ mouse model reproduces many of the histopathological characteristics associated with human gastric MALT lymphoma and therefore represents a practicable and pre-clinical model of MALT lymphomagenesis.

## CD40L antibody blockade reduces B-cell follicle formation in *H. felis*-infected *Nlrc5*$^{mø\text{-}KO}$ mice

CD40–CD40L signalling is a T-cell-dependent pathway that is required for B-cell proliferation and thus plays a pivotal role in B-cell MALT lymphoma development [12,31]. Previous studies reported contradictory findings regarding the role of CD40–CD40L interactions in B-cell MALT lymphoma development *in vitro* [12,13]. We investigated this question *in vivo* by injecting *Nlrc5*$^{mø\text{-}KO}$ mice intraperitoneally with either blocking anti-CD40L or IgG isotype control antibodies during establishment of *H. felis* infection (supplementary material, Figure S3A). These antibody treatments were continued until mice were culled at 3 months post-infection.

Remarkably, mice treated with the anti-CD40L antibody had significantly lower stomach and spleen weights (Figure 2A,B), but no change in either total body or mesenteric lymph node weights (supplementary material, Figure S10), compared with mice given the IgG isotype control. Moreover, anti-CD40L antibody treatment significantly reduced the level of gastric hyperplasia and lymphoid follicle numbers in the mice (Figure 2C–F). Importantly, none of the mice receiving the anti-CD40L treatment developed lymphoid follicles in the stomach (Figure 2E). mIHC analyses demonstrated that mice receiving the anti-CD40L treatment exhibited significantly lower numbers of CD19$^+$ B-cells, CD11c$^+$ DCs, F4/80$^+$ macrophages, CD4$^+$ and CD8$^+$ T-cells, and CD4$^+$Foxp3$^+$ Tregs in gastric tissues compared with control mice (Figure 2G–P). In contrast, the proportion of CD45$^+$ immune cells (CD4$^+$ and CD8$^+$ T-cells, B-cells, macrophages, DCs, and neutrophils) in the spleens and mesenteric lymph nodes did not differ between the anti-CD40L and control treatment groups (Figure 3A–F and supplementary material, Figure S11). These data show that treatment with anti-CD40L antibody significantly reduced gastric immune cell infiltration and B-cell formation in *Nlrc5*$^{mø\text{-}KO}$ mice with chronic *H. felis* infection.

Since gastric B-cell MALT lymphoma is strongly linked with *Helicobacter* infection, we sought to determine whether anti-CD40L blockade impacts *H. felis* colonisation in this mouse model. Interestingly, the anti-CD40L-treated mice had lower levels of stomach colonisation compared with control animals (Figure 3G and supplementary material, Figure S12). To confirm whether the reduced *H. felis* colonisation levels were directly impacted by anti-CD40L antibody administration, we assessed the bactericidal activities of the anti-CD40L and control IgG antibodies *in vitro*, used at the same concentration as in the intraperitoneal injections. No significant differences in the bactericidal activities of these antibodies were observed (Supplementary material, Figure S13), indicating that the reduced *H. felis* colonisation in the mouse stomach was not likely due to the direct actions of the anti-CD40L antibody. An alternative explanation is that anti-CD40L blockade might result in reduced B-cell activation and differentiation. Indeed, the levels of *Helicobacter*-specific IgG total and subclass antibodies were significantly reduced in mice treated with anti-CD40L antibody compared with control mice (Figure 3H–J). This result may, however,

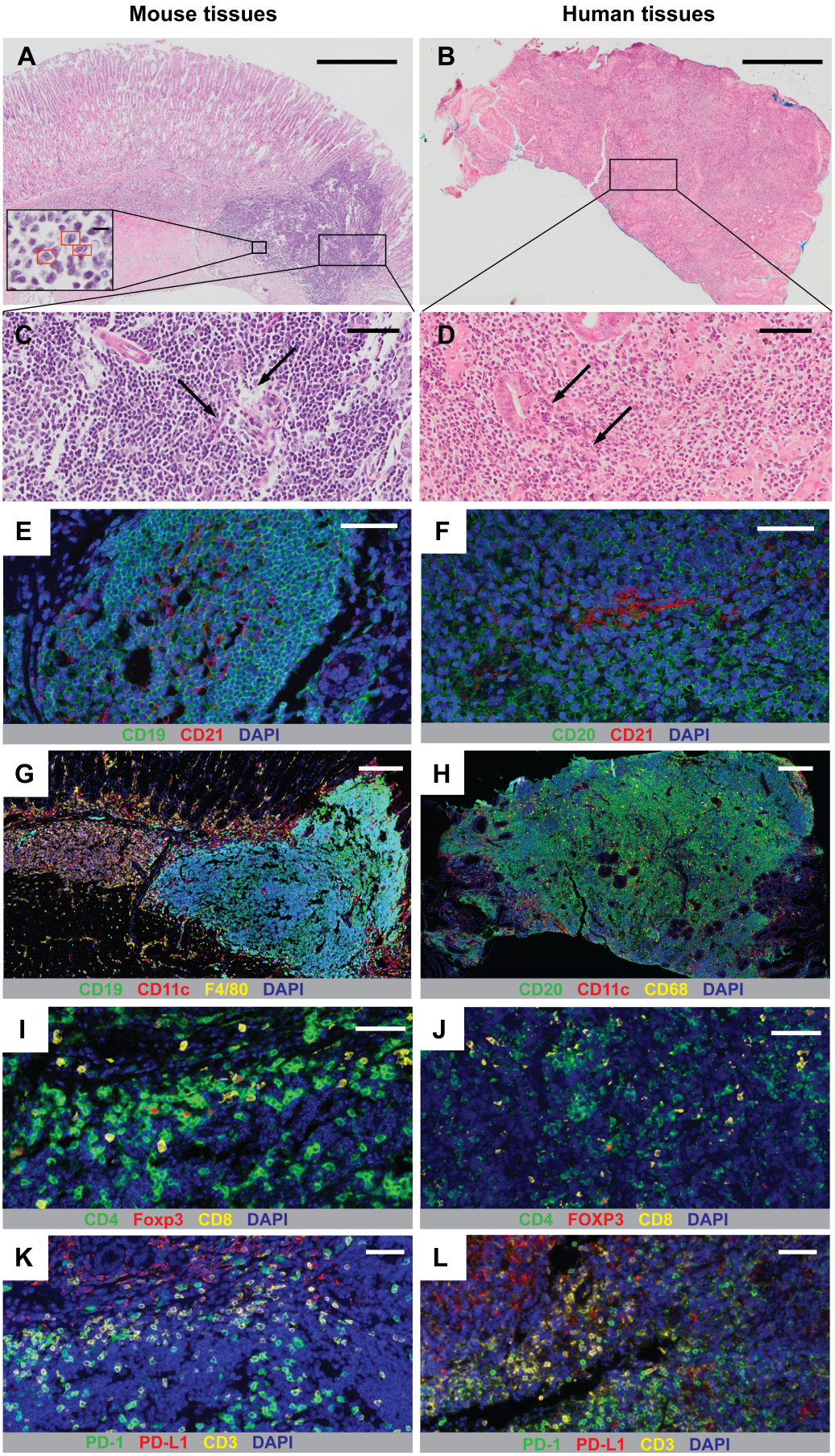


Figure 1 Legend on next page.

also reflect the different colonisation levels between the two groups of mice.

To elucidate the effect of the anti-CD40L treatment on host immune responses, we assessed the expression levels in gastric tissues of key immune genes associated with gastric MALT lymphomagenesis, including those regulating Th responses [19] and B-cell proliferation [20]. The expression levels of Th1 cytokine genes, interferon-γ (*Ifng*), interleukin-12 (*Il12*), and *Tnf*, in gastric tissues of anti-CD40L-treated mice were not significantly different to those in control mice (Figure 4A–C). In contrast, expression of the Th17 cytokine gene *Il17* was significantly reduced in tissues of mice receiving anti-CD40L antibody (Figure 4D), whereas the Th2 cytokine gene *Il4* was not detectable in tissues (data not shown). The expression levels of genes encoding mouse APRIL (*Tnfsf13*) and transmembrane activator and calcium-modulating cyclophilin ligand interactor (TACI; *Tnfrsf13b*), but not BAFF (*Tnfsf13b*), were significantly reduced in mice receiving anti-CD40L treatment compared with control animals (Figure 4E–G). Interestingly, we also observed decreased interferon regulatory factor 4 (*Irf4*) gene expression in the gastric tissues of anti-CD40L-treated mice (Figure 4H). *IRF4* was found to be aberrantly expressed in various types of B-cell non-Hodgkin lymphoma and is required for germinal centre formation [32].

Taken together, these data demonstrate that antibody blockade of CD40L significantly suppresses gastric B-cell MALT formation and reduces immune cell infiltration in *Nlrc5*$^{mø\text{-}KO}$ mice with chronic *Helicobacter* infection. In addition, the data identify Th17 responses and the B-cell-promoting factors, APRIL and TACI, as potential targets of anti-CD40L treatment in this model.

### Anti-CD40L antibody treatment prevents the formation of precursor lesions to gastric MALT lymphoma in mice with chronic *Helicobacter* infection

A monoclonal antibody that targets CD20 on B-cells (rituximab) has shown some effectiveness when used either alone or in combination with other chemotherapies as a therapeutic treatment for non-Hodgkin lymphomas [6], including gastric MALT lymphoma [33,34]. As the anti-CD40L antibody was highly effective in preventing gastric B-cell MALT lesions in mice during the establishment of *Helicobacter* infection (Figure 2), we sought to determine whether this antibody may also have activity against disease development in animals with chronic infection. For this, *Nlrc5*$^{mø\text{-}KO}$ mice were inoculated with *H. felis* bacteria and after 4 weeks, then injected intraperitoneally with either the anti-CD40L antibody or an IgG isotype control (supplementary material, Figure S3B). Mice were subsequently administered these antibodies weekly for a further 8 weeks.

Interestingly, anti-CD40L-treated mice exhibited no significant changes in stomach, spleen, or body weights compared with control mice receiving the IgG isotype control antibody (Figure 5A,B). A significant reduction in mesenteric lymph node weight was, however, found in the anti-CD40L-treated mice (supplementary material, Figure S14). Importantly, mice given anti-CD40L treatment also displayed a significant decrease in the levels of gastric lymphoid follicles and hyperplasia compared with control mice (Figure 5C–F). mIHC analyses demonstrated that the gastric tissues of anti-CD40L-treated mice had significantly reduced numbers of CD19$^+$ B-cells, CD11c$^+$ DCs, CD8$^+$ and Foxp3$^+$ T-cells but not macrophages, when compared with control mice (Figure 5G–P). Conversely, the spleens (Figure 6A–F) and mesenteric lymph nodes (supplementary material, Figure S15) of the two groups had similar numbers of CD45$^+$ immune cells (B-cells, DCs, macrophages, T-cells, and neutrophils).

Administration of anti-CD40L antibody in *H. felis*-infected mice had no significant effect on the levels of stomach colonisation (Figure 6G). This supports the suggestion that the observed reductions in *H. felis* colonisation reported in Figure 3G were not due to bactericidal effects of the antibody. Finally, we observed significantly reduced levels of *Helicobacter*-specific total IgG responses in the sera of mice receiving anti-CD40L treatment compared with the control mice (Figure 6H), though no significant differences were observed for IgG1 and IgG2c responses (Figure 6I,J).

Collectively, these data show that the administration of anti-CD40L antibody can attenuate the formation of precursor B-cell lesions to gastric MALT lymphoma in *Nlrc5*$^{mø\text{-}KO}$ mice with chronic *Helicobacter* infection. These findings further validate *Nlrc5*$^{mø\text{-}KO}$ mice as a practicable model to study this type of lymphoma.

## Discussion

Gastric B-cell MALT lymphoma is one of the most common types of extranodal non-Hodgkin lymphoma [19]. Here, we describe a new mouse model in which animals develop precursor B-cell lesions to gastric MALT lymphoma faster than in any existing model.

**Figure 1.** *Helicobacter*-infected *Nlrc5*$^{mø\text{-}KO}$ mice develop precursor lesions to gastric B-cell MALT lymphoma. Representative H&E-stained sections of gastric tissues from (A) *Nlrc5*$^{mø\text{-}KO}$ mice at 3 months post-infection with *H. felis* and (B) human subjects with *H. pylori*-associated MALT lymphoma. Red rectangles (inset in Figure 1A) indicate centrocyte-like cells. (C, D) Higher-magnification views of sections in A and B, respectively. Arrows indicate lympho-epithelial lesions. mIHC analyses of gastric tissues from (E, G, I, K) *Nlrc5*$^{mø\text{-}KO}$ mice and (F, H, J, L) human gastric MALT lymphoma subjects with *Helicobacter* infection. The cell markers used are as shown in each figure panel. (E, F) Detection of B-cells (green), CD21$^+$ cells (red), and nuclei (blue). (G, H) Detection of B-cells (green), CD11c$^+$ DCs (red), macrophages (yellow), and nuclei (blue). (I, J) Detection of CD4$^+$ T-cells (green), Foxp3/FOXP3$^+$ Tregs (red), CD8$^+$ T-cells (yellow), and nuclei (blue). (K, L) Detection of PD-1$^+$ cells (green), PD-L1$^+$ cells (red), CD3$^+$ T-cells (yellow), and nuclei (blue). Scale bar: 500 μm (A, B); 50 μm (C–F, I–L); 200 μm (G, H).

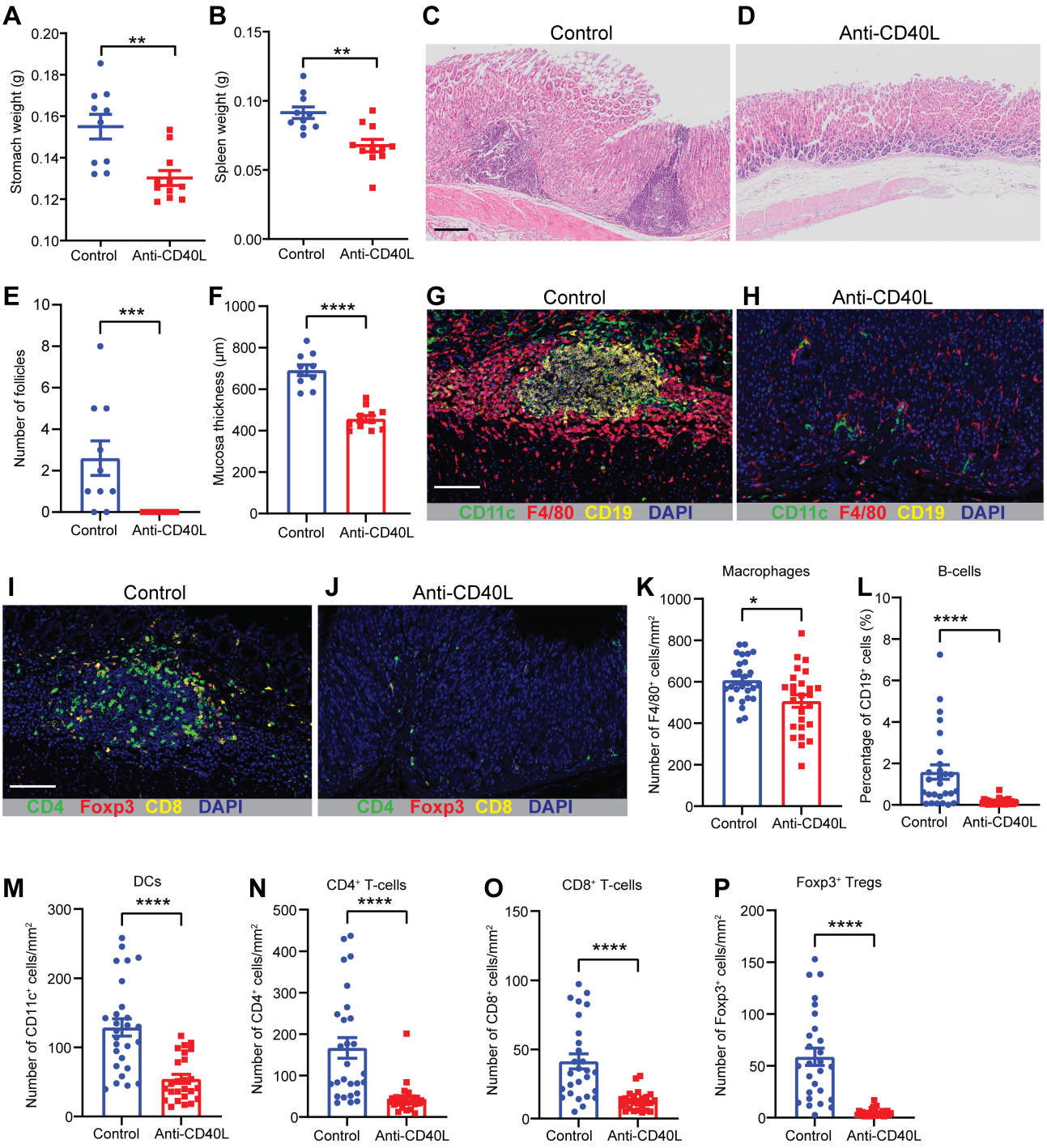


**Figure 2.** CD40L antibody blockade during *H. felis* infection attenuates B-cell MALT lesions and gastric hyperplasia. *Nlrc5*$^{mø\text{-}KO}$ mice administered anti-CD40L antibody concomitant with the infection process (supplementary material, Figure S3A; $n = 11$) had significantly reduced (A) stomach and (B) spleen weights compared with animals receiving an isotype control antibody ($n = 10$). Representative H&E-stained sections of gastric tissues from mice receiving either (C) control or (D) anti-CD40L blocking antibodies. The gastric tissues from mice in the anti-CD40L treatment group showed significantly reduced (E) B-cell follicles and (F) mucosal thickness compared with control animals. mIHC detection of CD11c$^+$ DCs (green), F4/80$^+$ macrophages (red), CD19$^+$ B-cells (yellow), and nuclei (blue) in the gastric tissues from mice receiving either (G) control or (H) anti-CD40L blocking antibodies. Detection of CD4$^+$ T-cells (green), Foxp3$^+$ Tregs (red), CD8$^+$ T-cells (yellow), and nuclei (blue) in the gastric tissue from mice receiving either (I) control or (J) anti-CD40L blocking antibodies. The gastric tissues of anti-CD40L-treated mice had significantly reduced numbers of (K) F4/80$^+$ macrophages, (L) CD19$^+$ B-cells, (M) CD11c$^+$ DCs, (N) CD4$^+$ T-cells, (O) CD8$^+$ T-cells, and (P) Foxp3$^+$ Tregs compared with control animals. Data are presented as the mean ± SEM. Mann–Whitney test; *$p < 0.05$, **$p < 0.01$, ***$p < 0.001$, ****$p < 0.0001$. Scale bar: 200 µm (C); 150 µm (G, I).

We have used this model to show for the first time that antibody blockade of CD40L prevents the formation of these lesions. We propose that CD40–CD40L signalling is a potential therapeutic target for the treatment of human gastric B-cell MALT lymphoma due to *H. pylori* infection.

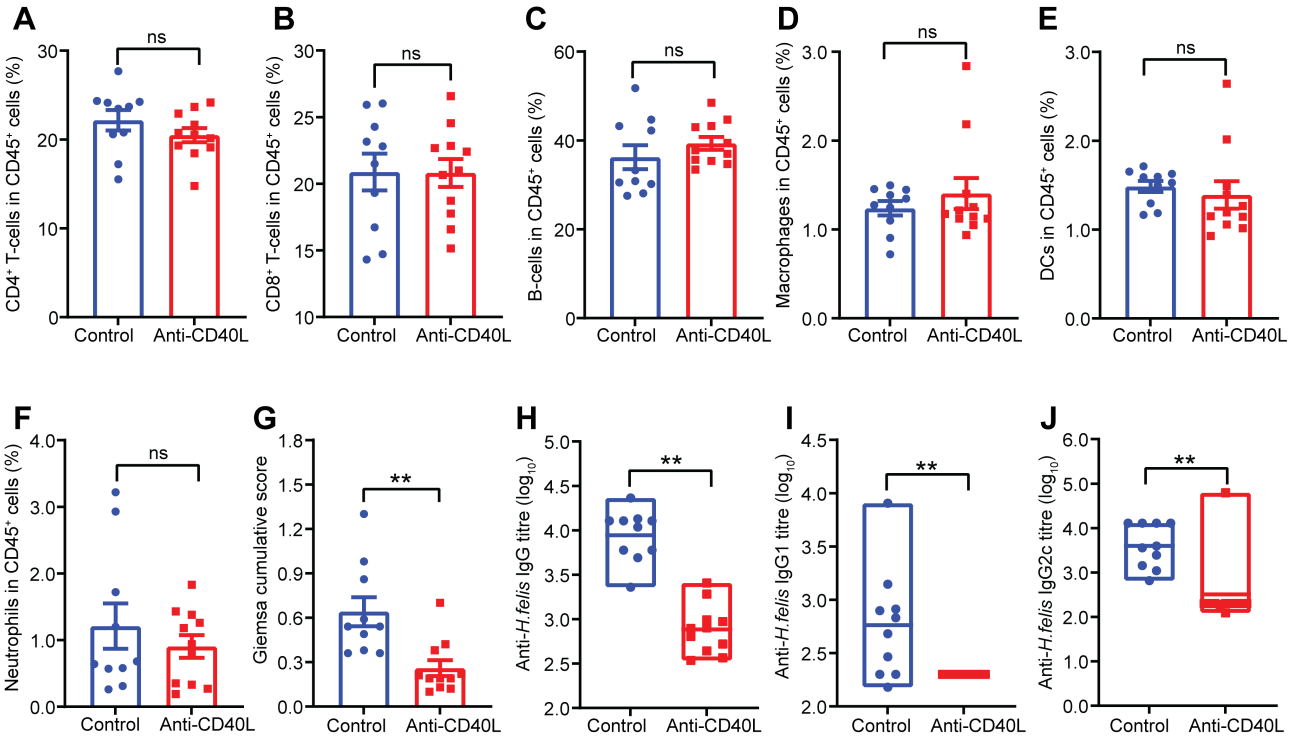


**Figure 3.** CD40L antibody blockade during *H. felis* infection affects colonisation and serum antibody responses. Flow cytometry on splenic CD45$^+$ cell populations from *Nlrc5*$^{mø\text{-}KO}$ mice receiving anti-CD40L blocking antibodies during the infection process (supplementary material, Figure S3A) showed no significant differences in the percentages of (A) CD4$^+$ T-cells, (B) CD8$^+$ T-cells, (C) B-cells, (D) macrophages, (E) DCs, or (F) neutrophils compared with animals receiving the control antibody. The anti-CD40L-treated mice exhibited significantly lower (G) *H. felis* colonisation scores and *Helicobacter*-specific (H) IgG, (I) IgG1, and (J) IgG2c titres compared with control animals. Data are presented as the mean ± SEM. Mann–Whitney test; $^{**}p < 0.01$. ns, not significant.

Consistent with previous work [35], most infiltrating T-cells in the gastric MALT microenvironment of *Nlrc5*$^{mø\text{-}KO}$ mice were CD4$^+$ T-helper cells, with a significant number of CD8$^+$ T-cells present across the gastric mucosa (Figure 1). This suggested that T-helper cells may play a more important role than cytotoxic T-cells in MALT lymphoma. We also detected PD-1 and PD-L1 expression in both mouse and human MALT lymphoid follicles (Figure 1). It was suggested that up-regulated PD-L1 expression may favour immune evasion and, consequently, the persistence of *H. pylori* infection and associated tumours [36]. Consistent with this idea, many subtypes of B-cell lymphoma, especially cases of refractory disease [30], showed increased levels of PD-1/PD-L1 expression [30,37]. Our results suggest that immune checkpoint inhibitors may be beneficial for the treatment of gastric MALT lymphoma patients with *Helicobacter* infection and, moreover, that *Nlrc5*$^{mø\text{-}KO}$ mice may serve as a pre-clinical model to test such therapies *in vivo*.

Drugs that target either CD40 or CD40L have been the subject of ongoing clinical trials for several autoimmune diseases, including rheumatoid arthritis [10]. However, there have been relatively few trials of drugs targeting CD40 for the treatment of human MALT lymphoma and, to our knowledge, none targeting CD40L. We show that administration of anti-CD40L antibody both prior to and after establishment of chronic *Helicobacter* infection significantly reduced the numbers of gastric B-cell follicles in *Nlrc5*$^{mø\text{-}KO}$ mice (Figure 2). Anti-CD40L treatment reshaped the local microenvironment, as characterised by decreased numbers of CD19$^+$ B-cells, CD8$^+$ T-cells, CD11C$^+$ DCs, and Foxp3$^+$ Tregs in gastric tissues (Figures 2 and 5). Conversely, the proportions of CD45$^+$ immune cells (CD4$^+$ and CD8$^+$ T-cells, B-cells, macrophages, DCs, and neutrophils) were unchanged in the secondary lymphoid organs of the animals (Figures 3 and 6). The observed inhibitory effect of anti-CD40L treatment on gastric B-cell lesions differs from the findings of a previous study which reported that an anti-CD40L blocking antibody did not inhibit proliferation of tumour B-cells from *H. felis*-infected mice in response to *H. felis* stimulation [13]. Interestingly, however, the depletion of CD40L$^+$ cells did result in reduced tumour cell proliferation [13]. Those experiments were performed in a tumour model using single-cell suspensions which were unable to reproduce the local tumour microenvironment and spatial context of immune cells present in primary tumours.

Several differences were observed between the two treatment regimens in this study. Notably, administration of anti-CD40L antibody before but not after establishment of *H. felis* infection resulted in significantly reduced stomach and spleen weights, and decreased levels of *H. felis* colonisation in the stomach (Figures 2 and 4G, respectively). The anti-CD40L antibody did not directly affect *H. felis* viability *in vitro* (supplementary material, Figure S13), suggesting that bacterial clearance could not be attributed to bactericidal effects of the anti-

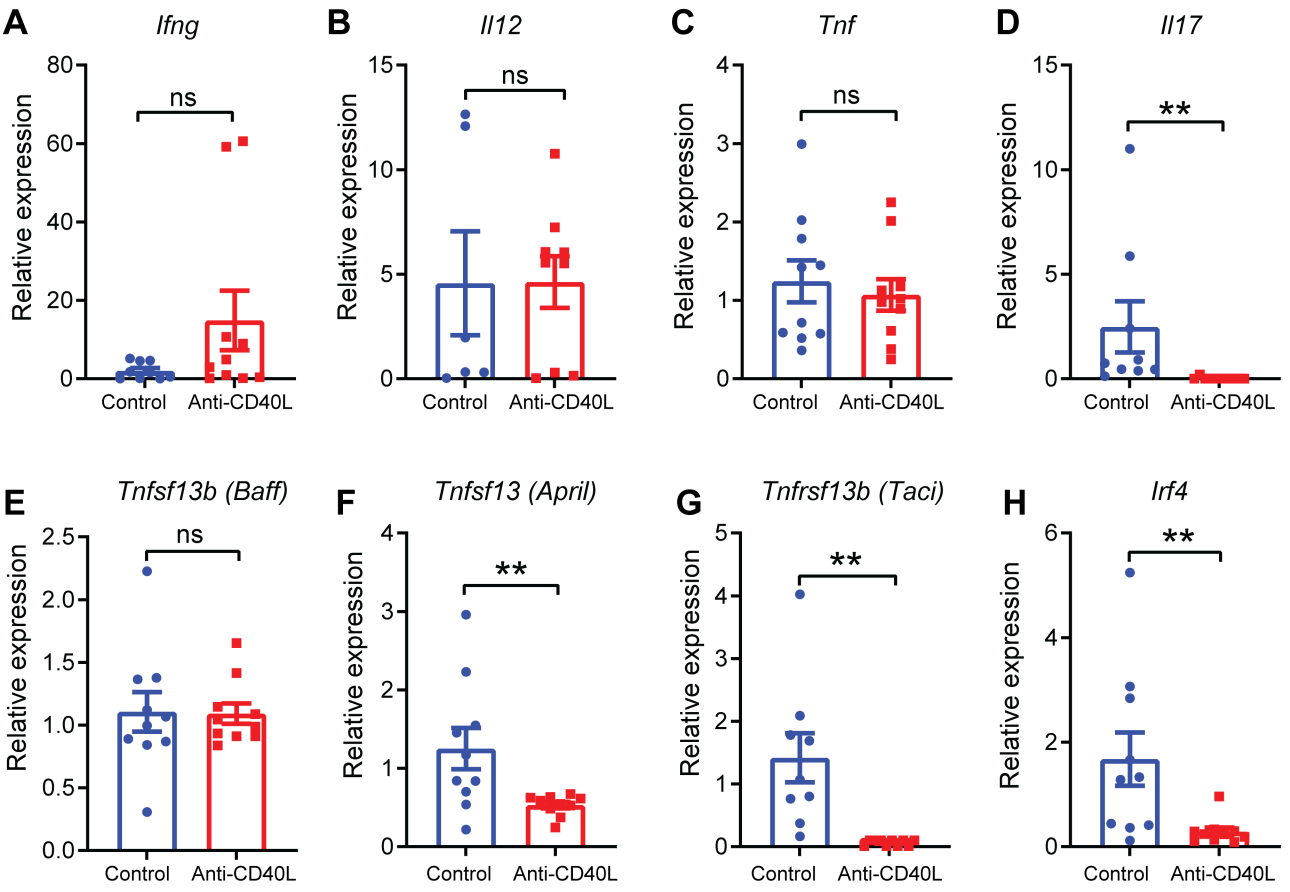


**Figure 4.** CD40L antibody blockade during *H. felis* infection results in decreased gastric expression levels of lymphoma-associated genes. Relative gene expression levels in gastric tissues of *Nlrc5*$^{mø\text{-}KO}$ mice receiving either anti-CD40L blocking or control antibodies during the infection process (supplementary material, Figure S3A). (A) *Ifng*, (B) *Il12*, (C) *Tnf*, (D) *Il17*, (E) *Tnfsf13b* (*Baff*), (F) *Tnfsf13* (*April*), (G) *Tnfrsf13b* (*Taci*), and (H) *Irf4*. Gene expression was normalised to that of *18S* ribosomal RNA. Data are presented as the mean ± SEM. Mann–Whitney test; $^{**}p < 0.01$. ns, not significant.

CD40L antibody but most likely occurred due to disrupted cross-talk between T- and B-cells required for anti-*Helicobacter* protective immunity. Treatment with the anti-CD40L antibody in mice with chronic *Helicobacter* infection suppressed B-cell MALT lesions independently of the levels of bacterial colonisation (Figure 6G), suggesting that anti-CD40L therapies might be useful for the treatment of gastric B-cell MALT lymphoma patients who are resistant to *H. pylori* eradication or relapse after its eradication.

Significantly reduced expression levels of *Il17* were detected in the gastric tissues from the mice receiving anti-CD40L treatment, whereas expression of Th1- and Th2-type cytokine genes was unaffected (Figure 4). Previous studies reported that gastric MALT lymphomas are infiltrated by Th2 cells [12,13], while one study found that IL-17 production was elevated in the stomachs of *H. felis*-infected mice with MALT lesions [38]. In an autoimmune encephalitis model, Th17 cell development was dependent on CD40–CD40L cross-talk [39], leading us to speculate that Th17-producing CD4$^{+}$ cells may be inhibited by the anti-CD40L treatment. However, as CD40L is also expressed by immune, epithelial, endothelial, and smooth muscle cells [40], further studies are required to identify the main cell type affected by the anti-CD40L therapy in our model.

We previously identified murine BAFF as promoting B-cell hyperproliferation in *Nlrc5*$^{mø\text{-}KO}$ mice [18]. Anti-CD40L treatment did not, however, affect the gastric expression levels of the corresponding gene. Soluble forms of BAFF and APRIL are secreted by macrophages and bind to TACI and BCMA receptors on B-cells to promote cell activation [21]. As BAFF exists as a transmembrane form on macrophages [41], it is possible that the expression of this form was not affected by the anti-CD40L treatment. Interestingly, expression levels for the genes encoding APRIL and TACI were reduced (Figure 4). APRIL has been suggested to play an important role in gastric MALT lymphomagenesis [42,43]. This survival factor is widely expressed by various cells, including immune, epithelial, and tumour cells. APRIL was also reported to be expressed by tumour-associated macrophages [42] and eosinophils in gastric MALT lymphoma [43], and could be induced by *H. pylori* antigen-specific T-cells [42]. We also showed that blocking the binding of CD40L to CD40 resulted in significant decreases in *Irf4* gene expression in gastric tissues (Figure 4). Consistent with this finding, a previous study showed

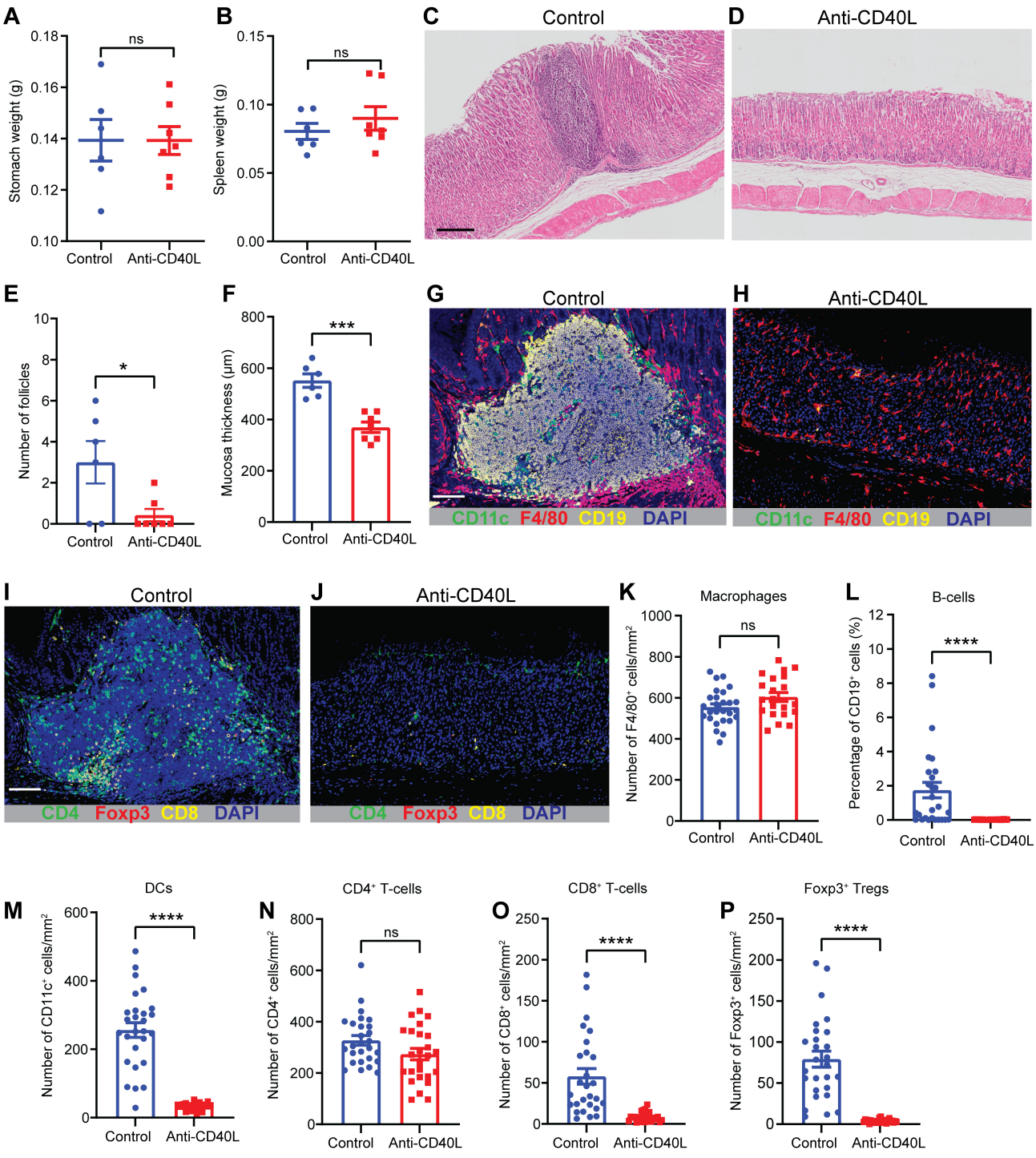


**Figure 5.** Anti-CD40L antibody treatment prevents gastric B-cell MALT lesion formation in mice with chronic *Helicobacter* infection. *Nlrc5*$^{mø\text{-}KO}$ mice with chronic *H. felis* infection that were administered anti-CD40L antibody (supplementary material, Figure S3B; $n = 7$) had (A) stomach and (B) spleen weights similar to those of control animals ($n = 6$). Representative H&E-stained sections of gastric tissues from mice receiving either (C) control or (D) anti-CD40L blocking antibodies. The gastric tissues from the mice in the anti-CD40L treatment group showed significantly reduced (E) B-cell follicle numbers and (F) mucosal thickness compared with those from control animals. mIHC detection of CD11c$^+$ DCs (green), F4/80$^+$ macrophages (red), CD19$^+$ B-cells (yellow), and nuclei (blue) in the gastric tissues from mice receiving either (G) control or (H) anti-CD40L blocking antibodies. Detection of CD4$^+$ T-cells (green), Foxp3$^+$ Tregs (red), CD8$^+$ T-cells (yellow), and nuclei (blue) in the gastric tissues from mice receiving either (I) control or (J) anti-CD40L blocking antibodies. Quantification in gastric tissues of (K) F4/80$^+$ macrophages, (L) CD19$^+$ B-cells, (M) CD11c$^+$ DCs, (N) CD4$^+$ T-cells, (O) CD8$^+$ T-cells, and (P) Foxp3$^+$ Tregs. Data are presented as the mean ± SEM. Mann–Whitney test; *$p < 0.05$, **$p < 0.01$, ***$p < 0.001$, ****$p < 0.0001$. and ns, not significant. Scale bar: 200 µm (C); 150 µm (G, I).

that *IRF4* expression was up-regulated by both soluble and membrane-bound CD40L in different Hodgkin lymphoma-derived cell lines [44].

In conclusion, we report that *Nlrc5*$^{mø\text{-}KO}$ mice represent a practicable, pre-clinical model of human gastric MALT lymphomagenesis. By using this mouse model,

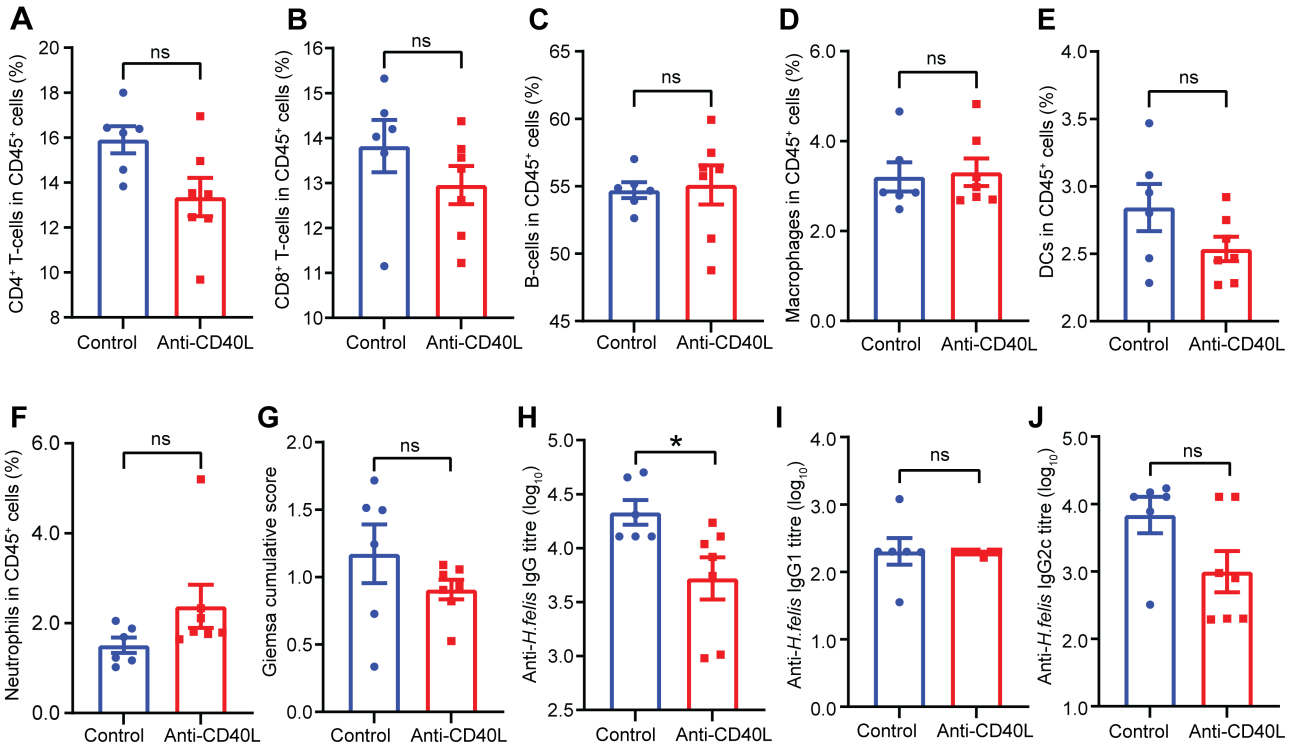


**Figure 6.** Anti-CD40L antibody treatment results in reduced serum IgG responses in mice with chronic *Helicobacter* infection. Flow cytometry on splenic CD45$^+$ cell populations from *Nlrc5*$^{mø\text{-}KO}$ mice with chronic *H. felis* infection receiving anti-CD40L blocking antibody (supplementary material, Figure S3B) showed no significant differences in the percentages of (A) CD4$^+$ T-cells, (B) CD8$^+$ T-cells, (C) B-cells, (D) macrophages, (E) DCs, or (F) neutrophils compared with animals receiving control antibody. The anti-CD40L-treated mice had (G) similar *H. felis* colonisation scores, (H) significantly reduced *Helicobacter*-specific serum IgG titres, but similar *Helicobacter*-specific serum (I) IgG1 and (J) IgG2c titres compared with control animals. Data are presented as the mean ± SEM. Mann–Whitney test; *$p < 0.05$. ns, not significant.

we show for the first time that the prevention of *Helicobacter*-induced precursor lesions to gastric B-cell MALT lymphoma can be achieved by anti-CD40L antibody blockade. These findings provide a rational basis for future research into the translational application of anti-CD40L drugs for the treatment of gastric B-cell MALT lymphomagenesis due to *Helicobacter* infection.

## Acknowledgements

This project in RLF's laboratory was supported by the US Department of Defense (Award No. W81XWH-17-1-0606), the National Health and Medical Research Council (Project grant APP1107930, Ideas grant APP2012620, and Senior Research Fellowship, APP1079904), and Tour de Cure (Sydney, Australia; RSP-330-2020). The Singapore Ministry of Health's National Medical Research Council (NMRC-OFLCG-18May0028), Tanoto Foundation (Professorship in Medical Oncology to STL), and the Ling Foundation are thanked for their support. We acknowledge the Monash Histology Platform (Monash University, Monash Health Translation Precinct) for assisting with tissue processing and scanning. We are grateful to Dr Feng Yan for critical discussion and feedback. Construction of the *Nlrc5*$^{fl/fl}$ mice was funded in part by the Public Health Agency of Canada. Research at the Hudson Institute of Medical Research is supported by the Victorian Government's Operational Infrastructure Support Program. Open access publishing facilitated by Monash University, as part of the Wiley - Monash University agreement via the Council of Australian University Librarians.

## Author contributions statement

LY performed experiments, analysed data and drafted the manuscript. PL, GW-M, JE, LST, NC, LHML and PX performed experiments. ZD conducted analyses and revised the manuscript. LY provided technical support and revised the manuscript. YT provided primary antibodies for mIHC staining and revised the manuscript. DJP provided reagents. DMZC prepared clinical samples. CLC, STL and CKO provided histopathological review of samples, clinical information and reviewed the manuscript. RLF designed the research, supervised the experiments and revised the manuscript.

## Data availability statement

All the data are included in the paper and online supplementary material.

## References


1. Raderer M, Kiesewetter B, Ferreri AJM. Clinicopathologic characteristics and treatment of marginal zone lymphoma of mucosa-associated lymphoid tissue (MALT lymphoma). *CA Cancer J Clin* 2016; **66:** 152–171.
2. Ferrucci PF, Zucca E. Primary gastric lymphoma pathogenesis and treatment: what has changed over the past 10 years? *Br J Haematol* 2007; **136:** 521–538.
3. Sagaert X, Van CE, De HG, *et al*. Gastric MALT lymphoma: a model of chronic inflammation-induced tumor development. *Nat Rev Gastroenterol Hepatol* 2010; **7:** 336–346.
4. Stathis A, Chini C, Bertoni F, *et al*. Long-term outcome following *Helicobacter pylori* eradication in a retrospective study of 105 patients with localized gastric marginal zone B-cell lymphoma of MALT type. *Ann Oncol* 2009; **20:** 1086–1093.
5. Nakamura S, Matsumoto T. Treatment strategy for gastric mucosa-associated lymphoid tissue lymphoma. *Gastroenterol Clin North Am* 2015; **44:** 649–660.
6. Morgner A, Schmelz R, Thiede C, *et al*. Therapy of gastric mucosa associated lymphoid tissue lymphoma. *World J Gastroenterol* 2007; **13:** 3554–3566.
7. Raderer M, Streubel B, Woehrer S, *et al*. High relapse rate in patients with MALT lymphoma warrants lifelong follow-up. *Clin Cancer Res* 2005; **11:** 3349–3352.
8. Smith CD, Gupta S, Sinn Chin Y, *et al*. Long term outcomes of gastric mucosa-associated lymphoid tissue lymphoma treated with radiotherapy: a multi-center retrospective cohort study. *Hematol Oncol* 2023; **41**: 71–77.
9. Conconi A, Martinelli G, Thiéblemont C, *et al*. Clinical activity of rituximab in extranodal marginal zone B-cell lymphoma of MALT type. *Blood* 2003; **102:** 2741–2745.
10. Karnell JL, Rieder SA, Ettinger R, *et al*. Targeting the CD40–CD40L pathway in autoimmune diseases: humoral immunity and beyond. *Adv Drug Deliv Rev* 2019; **141:** 92–103.
11. Hömig-Hölzel C, Hojer C, Rastelli J, *et al*. Constitutive CD40 signaling in B cells selectively activates the noncanonical NF-kappaB pathway and promotes lymphomagenesis. *J Exp Med* 2008; **205:** 1317–1329.
12. Greiner A, Knörr C, Qin Y, *et al*. Low-grade B cell lymphomas of mucosa-associated lymphoid tissue (MALT-type) require CD40-mediated signaling and Th2-type cytokines for *in vitro* growth and differentiation. *Am J Pathol* 1997; **150:** 1583–1593.
13. Craig VJ, Cogliatti SB, Arnold I, *et al*. B-cell receptor signaling and CD40 ligand-independent T cell help cooperate in *Helicobacter*-induced MALT lymphomagenesis. *Leukemia* 2010; **24:** 1186–1196.
14. Yamamoto K, Kondo Y, Ohnishi S, *et al*. The TLR4–TRIF–type 1 IFN–IFN-γ pathway is crucial for gastric MALT lymphoma formation after *Helicobacter suis* infection. *iScience* 2021; **24:** 103064.
15. Chrisment D, Dubus P, Chambonnier L, *et al*. Neonatal thymectomy favors *Helicobacter pylori*-promoted gastric mucosa-associated lymphoid tissue lymphoma lesions in BALB/c mice. *Am J Pathol* 2014; **184:** 2174–2184.
16. Floch P, Izotte J, Guillemaud J, *et al*. A new animal model of gastric lymphomagenesis: APRIL transgenic mice infected by *Helicobacter* species. *Am J Pathol* 2017; **187:** 1473–1484.
17. Yang L, Yamamoto K, Nishiumi S, *et al*. Interferon-γ-producing B cells induce the formation of gastric lymphoid follicles after *Helicobacter suis* infection. *Mucosal Immunol* 2015; **8:** 279–295.
18. Chonwerawong M, Ferrand J, Chaudhry HM, *et al*. Innate immune molecule NLRC5 protects mice from *Helicobacter*-induced formation of gastric lymphoid tissue. *Gastroenterology* 2020; **159:** 169–182.e8.
19. Kuo S-H, Wu M-S, Yeh K-H, *et al*. Novel insights of lymphomagenesis of *Helicobacter pylori*-dependent gastric mucosa-associated lymphoid tissue lymphoma. *Cancers (Basel)* 2019; **11:** 547.
20. Lee S-M, Kim E-J, Suk K, *et al*. BAFF and APRIL induce inflammatory activation of THP-1 cells through interaction with their conventional receptors and activation of MAPK and NF-κB. *Inflamm Res* 2011; **60:** 807–815.
21. Yang S, Li J-Y, Xu W. Role of BAFF/BAFF-R axis in B-cell non-Hodgkin lymphoma. *Crit Rev Oncol Hematol* 2014; **91:** 113–122.
22. D'Costa K, Chonwerawong M, Tran LS, *et al*. Mouse models of *Helicobacter* infection and gastric pathologies. *J Vis Exp* 2018; **(140):** 56985.
23. Bankhead P, Loughrey MB, Fernández JA, *et al*. QuPath: open source software for digital pathology image analysis. *Sci Rep* 2017; **7:** 16878.
24. Viala J, Chaput C, Boneca IG, *et al*. Nod1 responds to peptidoglycan delivered by the *Helicobacter pylori cag* pathogenicity island. *Nat Immunol* 2004; **5:** 1166–1174.
25. Chonwerawong M, Avé P, Huerre M, *et al*. Interferon-γ promotes gastric lymphoid follicle formation but not gastritis in *Helicobacter*-infected BALB/c mice. *Gut Pathog* 2016; **8:** 61.
26. Ying L, Yan F, Meng Q, *et al*. PD-L1 expression is a prognostic factor in subgroups of gastric cancer patients stratified according to their levels of CD8 and FOXP3 immune markers. *Oncoimmunology* 2018; **7:** e1433520.
27. Ferrero RL, Avé P, Radcliff FJ, *et al*. Outbred mice with long-term *Helicobacter felis* infection develop both gastric lymphoid tissue and glandular hyperplastic lesions. *J Pathol* 2000; **191:** 333–340.
28. Nakamura S, Ponzoni M. Marginal zone B-cell lymphoma: lessons from Western and Eastern diagnostic approaches. *Pathology* 2020; **52:** 15–29.
29. Xerri L, Chetaille B, Seriari N, *et al*. Programmed death 1 is a marker of angioimmunoblastic T-cell lymphoma and B-cell small lymphocytic lymphoma/chronic lymphocytic leukemia. *Hum Pathol* 2008; **39:** 1050–1058.
30. Xu-Monette ZY, Zhou J, Young KH. PD-1 expression and clinical PD-1 blockade in B-cell lymphomas. *Blood* 2017; **131:** 68–83.
31. Nakamura S, Matsumoto T. *Helicobacter pylori* and gastric mucosa-associated lymphoid tissue lymphoma: recent progress in pathogenesis and management. *World J Gastroenterol* 2013; **19:** 8181–8187.
32. Tsuboi K, Iida S, Inagaki H, *et al*. MUM1/IRF4 expression as a frequent event in mature lymphoid malignancies. *Leukemia* 2000; **14:** 449–456.
33. Martinelli G, Laszlo D, Ferreri AJM, *et al*. Clinical activity of rituximab in gastric marginal zone non-Hodgkin's lymphoma resistant to or not eligible for anti-*Helicobacter pylori* therapy. *J Clin Oncol* 2005; **23:** 1979–1983.
34. Salar A, Domingo-Domenech E, Panizo C, *et al*. Long-term results of a phase 2 study of rituximab and bendamustine for mucosa-associated lymphoid tissue lymphoma. *Blood* 2017; **130:** 1772–1774.
35. Mueller A, O'Rourke J, Chu P, *et al*. The role of antigenic drive and tumor-infiltrating accessory cells in the pathogenesis of *Helicobacter*-induced mucosa-associated lymphoid tissue lymphoma. *Am J Pathol* 2005; **167:** 797–812.
36. Silva R, Gullo I, Carneiro F. The PD-1:PD-L1 immune inhibitory checkpoint in *Helicobacter pylori* infection and gastric cancer: a comprehensive review and future perspectives. *Porto Biomed J* 2016; **1:** 4–11.
37. Panjwani PK, Charu V, DeLisser M, *et al*. Programmed death-1 ligands PD-L1 and PD-L2 show distinctive and restricted patterns of expression in lymphoma subtypes. *Hum Pathol* 2018; **71:** 91–99.
38. Zhao Y, Lu F, Ye J, *et al*. Myeloid-derived suppressor cells and γδT17 cells contribute to the development of gastric MALT lymphoma in *H. felis*-infected mice. *Front Immunol* 2020; **10:** 3104.
39. Iezzi G, Sonderegger I, Ampenberger F, *et al*. CD40–CD40L cross-talk integrates strong antigenic signals and microbial stimuli to induce development of IL-17-producing $CD4^+$ T cells. *Proc Natl Acad Sci U S A* 2009; **106:** 876–881.
40. Loskog A, Tötterman TH. CD40L – a multipotent molecule for tumor therapy. *Endocr Metab Immune Disord Drug Targets* 2007; **7:** 23–28.

41. Mackay F, Sierro F, Grey ST, *et al*. The BAFF/APRIL system: an important player in systemic rheumatic diseases. *Curr Dir Autoimmun* 2005; **8:** 243–265.
42. Munari F, Lonardi S, Cassatella MA, *et al*. Tumor-associated macrophages as major source of APRIL in gastric MALT lymphoma. *Blood* 2011; **117:** 6612–6616.
43. Blosse A, Peru S, Levy M, *et al*. APRIL-producing eosinophils are involved in gastric MALT lymphomagenesis induced by *Helicobacter* sp infection. *Sci Rep* 2020; **10:** 1–10.
44. Aldinucci D, Rapana B, Olivo K, *et al*. IRF4 is modulated by CD40L and by apoptotic and anti-proliferative signals in Hodgkin lymphoma. *Br J Haematol* 2010; **148:** 115–118.
45. Desar IME, van Deuren M, Sprong T, *et al*. Serum bactericidal activity against *Helicobacter pylori* in patients with hypogammaglobulinaemia. *Clin Exp Immunol* 2009; **15:** 434–439.

Reference 45 is cited only in supplementary material.

## SUPPLEMENTARY MATERIAL ONLINE

**Figure S1.** Representative H&E staining images showing the presence of *Helicobacter pylori* in human gastric MALT lymphoma biopsies

**Figure S2.** H&E staining of five human gastric tissues from gastric MALT lymphoma patients

**Figure S3.** Experimental protocol

**Figure S4.** Gating strategy for flow cytometry

**Figure S5.** Detection of $IgM^+$ cells (red) in gastric tissues of mice with MALT lymphoma lesions

**Figure S6.** Detection of $Ki67^+$ cells (brown) in gastric tissues of mice with MALT lymphoma lesions

**Figure S7.** Multiplex immunofluorescence histochemistry (mIHC) staining of DCs, macrophages, and B-cells in mouse and human gastric tissues

**Figure S8.** The relative abundance of $CD4^+$ and $CD8^+$ T-cells to $Foxp3^+$ cells in mouse and human gastric tissues with MALT

**Figure S9.** Detection of $CD4^+$ T-cells (green) and $Foxp3^+$ cells (red) in mouse gastric tissues with MALT lymphoma lesions

**Figure S10.** The anti-CD40L-treated mice showed (A) body and (B) mesenteric lymph node weights similar to those of control animals in the prophylactic model

**Figure S11.** The proportions of $CD45^+$ immune cells in the mesenteric lymph nodes of $Nlrc5^{mø\text{-}KO}$ mice receiving anti-CD40L treatment prophylactically were similar to those in control mice

**Figure S12.** Giemsa staining scoring of *H. felis* colonisation in mouse gastric tissues

**Figure S13.** The bactericidal effects of anti-CD40L antibody on *H. felis* viability

**Figure S14.** The anti-CD40L-treated mice showed mesenteric lymph node weights similar to those of control animals in the therapeutic model

**Figure S15.** The proportions of $CD45^+$ immune cells in the mesenteric lymph nodes of $Nlrc5^{mø\text{-}KO}$ mice receiving anti-CD40L treatment therapeutically were similar to those in control mice

**Table S1.** Antibody information for immunohistochemistry

**Table S2.** Antibody information for flow cytometry analyses

**Table S3.** Primer sequences used for qPCR

**Table S4.** Taqman probes used for qPCR

**Table S5.** The numbers of centrocyte-like cells in naïve mice and mice with MALT lymphoma